JOURNAL OF APPLIED ELECTROCHEMISTRY **27** (1997) 643–650

Study of gold deposition on copper by electrochemical and microscopic techniques

Y. G. LI, A. LASIA

Département de Chimie, Université de Sherbrooke, Sherbrooke, Canada, J1K 2R1

Received 26 February 1996; revised 21 October 1996

Deposition of gold on copper from acid gold bath was investigated using electrochemical and microscopic techniques. The growth morphology of both soft and hard gold deposits was characterized using scanning electron microscopy (SEM) and atomic force microscopy (AFM). Analysis of chronoamperometric transients showed that the mechanism of nucleation and growth of hard gold is three-dimensional progressive nucleation and growth of right-circular cones. This was further confirmed by SEM and AFM measurements. The grain size of hard gold deposit was shown to be much smaller than that of soft gold, indicating that nickel in deposit acts as a grain refiner. The mean roughness of hard gold deposit increases with deposition time, and with an increase of negative potential from –0.5 to –0.70 V (vs SCE), however, the surface becomes more uniform at –0.80 V. Similarly, the maximum height of clusters increases as potential is made more negative between –0.50 and –0.65 V, while it decreases steeply at potentials from –0.65 to –0.80 V. The inhibition of crystal growth in gold deposition at certain potentials was observed electrochemically and corroborated by microscopic techniques.

1. Introduction

Hard gold deposits are extensively used as electric contacts, connectors, in printed circuit boards, etc., due to their unique combination of physical and electrical properties [1–22]. Recently, a study was performed in this laboratory involving the mechanism and kinetics of gold deposition from a commercially used proprietary acid solution (Renovel N bath) [23–25]. The nucleation and growth mechanism in the initial stages of both soft and hard gold deposition on Au substrate was studied by analysing current–time transients [24, 25]. Two types of inhibition phenomena were observed in gold deposition under potentiostatic conditions. At more positive potentials, time-independent inhibition of crystal growth occurs in both soft and hard gold deposition, nucleation and crystal growth may be described by three dimensional nucleation and growth of right-circular cones. At more negative potentials a time-dependent partial inhibition process for crystal growth was observed in hard gold deposition, the process could be described by a modified Bosco–Rangarajan inhibition model [25].

SEM, transmission electron microscopy and X-ray diffraction techniques have been widely used in morphological studies of gold deposits [10, 11, 14, 18, 19]. Atomic force microscopy (AFM) was mainly used as an *in situ* method to monitor the growth morphology during metal electrodeposition [26–36] but there are no publications dealing with AFM of gold deposits. In recent years, deposition of copper [26–31], lead [32], silver [33], etc., was successfully studied *in situ* by AFM. However, artifacts introduced by AFM due to the interaction between the tip and substrate were also reported [28, 33, 37]. Besides its applications as an *in situ* method for electrochemical studies, AFM was also widely used as an *ex situ* method for morphological observation of the surface structure from nanometre to micrometre scales [34–36].

In the present work, the mechanism of nucleation and growth of gold on copper substrates were studied using linear sweep voltammetry and chronoamperometry. AFM and SEM were used *ex situ* to evaluate gold morphology under different conditions. The influence of deposition time and potential on morphology, surface roughness and grain size is described.

2. Experimental details

The supporting electrolyte used consisted of 75% (by volume) of a proprietary citrate-based buffer solution (Renovel N make-up solution, Lea Ronal) and 25% of deionized water. A current density extender (principally nicotinamide) was contained in the bath [20]. Two solutions were studied, that is, soft gold bath and hard gold bath. The soft gold bath contained 0.091 M Au as $KAu(CN)_2$ and hard gold bath contained the same quantity of gold and 0.027 M of nickel (as a proprietary nickel complex, Lea Ronal). A few measurements were also performed in a supporting electrolyte with and without addition of nickel complex. The pH was adjusted to 4.4. Deionized water (Barnstead, Nanopure) was used. Details of the pre-

0021-891X

paration of solutions were given elsewhere [23]. The working temperature was $60 \pm 0.5\,^{\circ}C$ and the solution was purged with nitrogen for at least 2 h prior to each measurement.

A potentiostat PAR Model M263 controlled by M270 software was employed. A three-compartment cell was used, the counter electrode being separated from the cathodic compartment by a Nafion® (Dupont) membrane to avoid the contamination by anodic products. The reference electrode was a saturated calomel electrode (SCE) and a Pt mesh was used as a counter electrode. A home-made copper rotating disc electrode (RDE) (0.071 cm^2, purity 99.995%), embedded in a Teflon holder, was used as a working electrode in linear sweep voltammetric and chronoamperometric experiments. It was polished with 1 and 0.05 μm Al_2O_3 to a mirror-like surface and rinsed thoroughly with water prior to each measurement. The rotator was of AFASR type (Pine). The distance between the RDE and the reference probe was set constant to give a constant solution resistance measured by a.c. impedance. As a substrate for morphological studies, a copper disc (1.0 cm^2 in area, 1.0 mm in height) was used. It was pretreated in series of steps starting with polishing with the finest sandpaper to remove mechanical scratches, polishing with 1 and 0.05 μm Al_2O_3 to a mirror-like surface, washing thoroughly with water, mounting into a special designed Teflon holder, which permitted fast changing of the plated samples, degreasing with methanol and, finally, washing again thoroughly with water. The disc surface was kept wet to diminish possibility of surface oxidation. To avoid an exchange reaction with gold, the initial immersion potential was set to –0.20 V (vs SCE). After deposition, the gold-plated copper disc was disconnected from the holder, degreased with methanol, washed thoroughly with water and dried in air as a sample for morphology characterization. JSM-840A scanning electron microscope was used in SEM measurements and Nanoscope III (Digital Instruments) was used in AFM studies, in a contact mode. All AFM measurements were performed in air at ambient temperature.

3. Results

3.1. *Linear sweep voltammetric measurements*

Figure 1 shows linear sweep voltammograms (LSV) recorded at a sweep rate of 1 mV s^{-1} for hard gold deposition on copper RDE at different rotation rates. There are two peaks on LSVs. The peak in the potential range between –0.50 V and –0.775 V increases with increasing rotation speed. Similar behaviour was also observed for gold deposition on Au [23], Ni and glassy carbon substrates (not shown here), although the magnitudes of peak height and the shape of LSV are different due to the nature of substrates. Such a peak-like behaviour observed in all substrates is probably associated with the reduction of AuCN

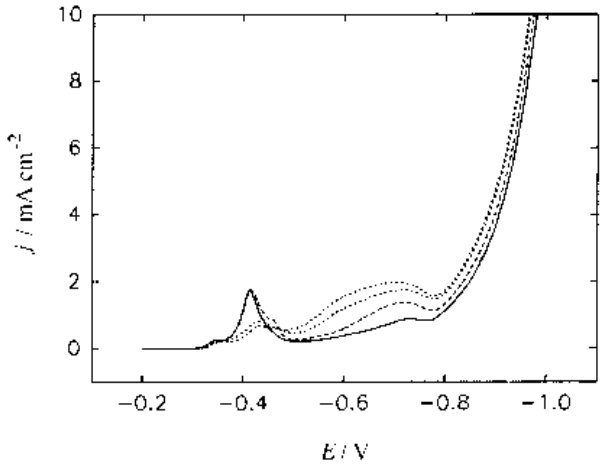

Fig. 1. Linear sweep voltammograms of hard gold deposition (in the presence of nickel) on Cu substrate at different rotation rates: (——) 650, (– – –) 1300, (– – –) 2700 and (· · · · ·) 4000 rpm. Sweep rate 1 mV s^{-1}.

adsorbed on the surface at less negative potentials [24, 25], rather than the direct reduction of $Au(CN)_2^-$ from bulk solution, that is, this feature is apparent irrespective of the diffusion of $Au(CN)_2^-$ because the observed current is much lower than that predicted by the Levich equation. In this potential range, gold deposition occurs via adsorption of AuCN followed by a charge-transfer reaction [11],

$$Au(CN)_2^- + H^+ \rightleftharpoons AuCN_{ads} + HCN \qquad (1)$$

$$AuCN_{ads} + H^+ + e^- \longrightarrow Au + HCN \qquad (2)$$

The production of HCN in Equation 2 has a very important effect on the whole process, especially when its initial concentration in the solution is sufficiently low as in acid solution. The dependence of current peak on rotation speed may be attributed to the mass transfer of cyanide species from the RDE surface to bulk solution since the initial concentration of free cyanide species in acid solution is extremely small. The observed current is proportional to the coverage of electroactive species AuCN. At higher rotation speed, the mass transfer of HCN from RDE to solution should be faster, leading to a higher coverage of electroactive species AuCN, Equation 1, and a higher current.

As the potential becomes more negative than –0.775 V, the current increases abruptly. At more negative potentials, similar to other substrates such as Au [23], Ni and glassy carbon, gold deposition in this range takes place predominately via a direct electron transfer mechanism [11],

$$Au(CN)_2^- + 2H^+ + e^- \longrightarrow Au + 2HCN \qquad (3)$$

Therefore, currents recorded at more negative potentials would be expected to increase on increasing overpotential, as illustrated in Fig. 1. The competition between reductions of AuCN adsorbed on the surface and soluble species $Au(CN)_2^-$ may take place at intermediate potentials. At more negative potentials, the hydrogen evolution reaction (HER) may occur simultaneously with gold deposition. No lim-

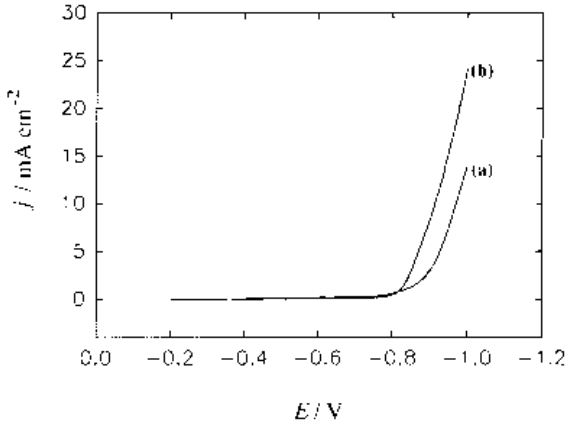

Fig. 2. Linear sweep voltammograms in the supporting electrolyte (a) and the supporting electrolyte containing 0.0273 M Ni^{2+} (b). Sweep rate 1 mV s^{-1}; rotation rate 650 rpm.

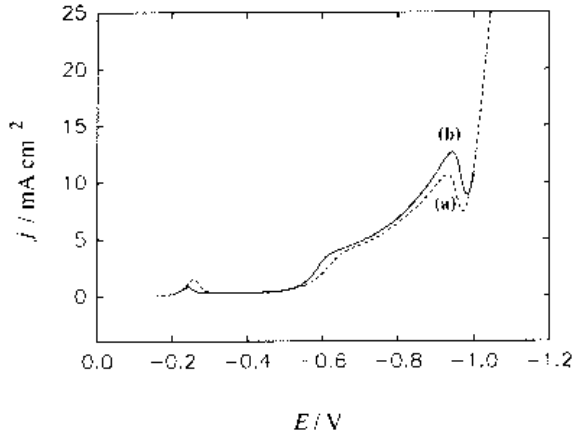

Fig. 3. Linear sweep voltammograms of soft gold deposition (in the absence of nickel) on Cu. Sweep rate 1 mV s^{-1}; rotation rate: (a) 1000 and (b) 2700 rpm.

iting current plateau was observed even at very negative potentials due to the onset of HER.

It is not clear yet what caused the peak (together with some small shoulders) at potentials around –0.4 V. The peak was not observed in the case of deposition on Au [23], Ni and glassy carbon substrates. The peak height seems to decrease with increasing rotation rate. It could be caused by the reduction of trace amount of oxide on the Cu substrate, the adsorption of organic additives, cyanide species or gold cyanide. In order to understand the possible reasons, LSV measurements were undertaken in the supporting electrolyte with and without addition of nickel complex, and in the soft gold plating solution (without nickel complex). LSV curves taken in the supporting electrolyte in the absence and presence of nickel complex show a similar feature, current increases at potentials more negative than about –0.7 V due to the hydrogen evolution reaction (HER) and no peak is observed, Fig. 2. These results suggest that the peak occurring at about –0.35 V on LSV in hard gold solution (Fig. 1) is caused neither by the reduction of trace amounts of oxide on Cu substrate, nor by the adsorption of organic additives in the supporting electrolyte and the nickel complex. Figure 3 illustrates LSVs on Cu RDE in soft gold solution, a small peak is also observed at about –0.25 V, and shifts in the positive direction in comparison with hard gold solution (Fig. 1). It is possible that such a small peak observed in soft and hard gold solution is connected to the adsorption of gold cyanide or other cyanide species. The possibility of CN^-/HCN adsorption causing peak formation can be discarded because the LSV measurements performed in supporting electrolyte containing 0.01 M KCN do not show such a feature. Therefore, it is reasonable to assume that the adsorption of gold cyanide produces small peak appearing at about –0.25 to –0.4 V.

3.2. *Chronoamperometric behaviour of hard gold deposition on Cu substrate*

Figure 4 illustrates typical chronoamperometric curves for hard gold deposition on Cu RDE at 2700 rpm. Two distinct features were observed in two potential ranges, indicating different nucleation and growth mechanisms. At potentials between –0.55 V and –0.70 V, the current initially falls to a minimum and, subsequently, increases to a quasi-plateau as a result of nucleation and crystal growth. The current measured at initial minimum increases with overpotential. The time, t_{min}, at which the minimum appears, is of the order of 40 s. The initial current fall

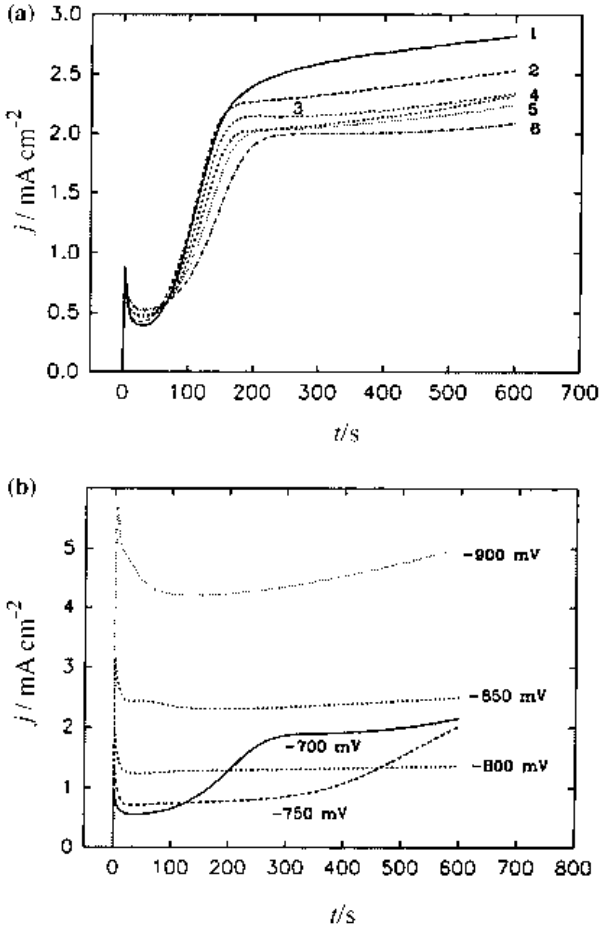

Fig. 4. Chronoamperometric curves of hard gold deposition on Cu. Rotation rate: 2700 rpm. Potentials used in Fig. 4(a) are: (1) −550, (2) −575, (3) −600, (4) −625, (5) −650 and (6) −675 mV.

could be attributed to three processes, that is, a double-layer charging, a transient diffusion process prior to a steady-state on a rotating disc electrode, and a direct deposition of metal without nucleation [24, 25]. However, the time required for the first two processes is less than a millisecond, therefore, other process(es) must be responsible for the initial current fall. It was postulated previously [24, 25] that gold deposition may take place prior to the minimum, after which a three-dimensional nucleation and crystal growth process starts. The use of Cu substrate enables us to verify this hypothesis. When the measurements were performed prior to the minimum, a gold deposit was clearly seen on the Cu substrate, indicating that deposition actually occurs before t_{min}. The charge consumed up to the minimum corresponds to about 80 compact gold monolayers. Thus, gold deposition may occur before the three-dimensional nucleation and crystal growth. At later stages, current increases and reaches a quasi-plateau. Such a behaviour may result from a three-dimensional nucleation and growth of right-circular cones. It was found that the height of the quasi-plateau decreases as the potential changes from –0.55 to –0.70 V, as shown in Fig. 4. The shape of the current–time transients is similar to that observed in the case of deposition on Au substrate [25]. It was found earlier [25] that in such conditions a three-dimensional progressive nucleation and growth of right-circular cones is involved in hard gold deposition on Au substrate. Accordingly, the current for this process is given as [25]:

$$i = zFk_0 \exp\left(-\frac{\pi M^2 k^2 A_{3D}}{3\rho^2} t^3\right) + zFk'\left[1 - \exp\left(-\frac{\pi M^2 k^2 A_{3D}}{3\rho^2} t^3\right)\right] \quad (4)$$

where k_0 is the outward growth rate constant for the substrate base plane (mol cm^{-2} s^{-1}), k' and k are the growth rate constants of right-circular cones in the directions perpendicular and parallel to the substrate (mol cm^{-2} s^{-1}), respectively, A_{3D} is the nucleation rate (nuclei cm^{-2} s^{-1}), M is the atomic weight (g) and ρ the density (g cm^{-3}) of gold.

The experimental data obtained at potentials from –0.55 to –0.70 V, Fig. 4, were fitted to Equation 4, and the results are illustrated in Fig. 5. The fit to a three-dimensional instantaneous nucleation and growth model was rejected on the basis of the statistical comparison. From these approximations, kinetic parameters for nucleation and growth may be obtained. The dependence of k_0 and k' on potential is given in Fig. 6. It is obvious that the rate constant, k_0, increases as potential is made more negative. However, the vertical growth rate constant, k', for three-dimensional growth of right-circular cones decreases with negative potentials, contrary to a typical case of exponential growth with overpotential [38], indicating an inhibition process. Such an abnormal growth was first found in gold deposition on Au substrates [24, 25]. The self-inhibition of gold deposition caused by the adsorption of CN^- or other CN^- containing species was suggested earlier by Davidović and Adzić [17]. Figure 7 shows a potential dependence of the combination of the lateral growth rate constant and the nucleation rate, k^2A_{3D}. The combined constant initially increases, and then decreases with negative potential. The results obtained above indicate that an inhibition of growth occurs in gold deposition.

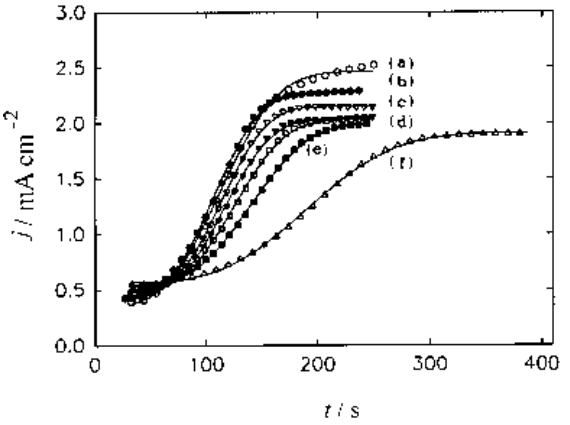

Fig. 5. Initial portion of current–time transients shown in Fig. 4 at potentials between –0.55 V and –0.70 V. Points: experimental data; solid line: theoretical fit to Equation 4. Potentials. (a) –550, (b) –575, (c) –600, (d) –625, (e) –650 and (f) –675 mV.

At potentials more negative than –0.75 V, the plateau-like behaviour of current–time transients disappears. The current falls to a steady-state at longer times. The shape of the curves recorded in this potential range is different from that for hard gold deposition on Au substrate [25], where a maximum, followed by a quasi steady-state, forms on the current transients. Furthermore, at very negative potentials, the initial current fall is accompanied by a shoulder, which was also observed in the case of Au substrate. We were unable to analyse the current–time transients recorded at potentials more negative than –0.75 V in view of nucleation and growth models since no well defined features were observed on these transients.

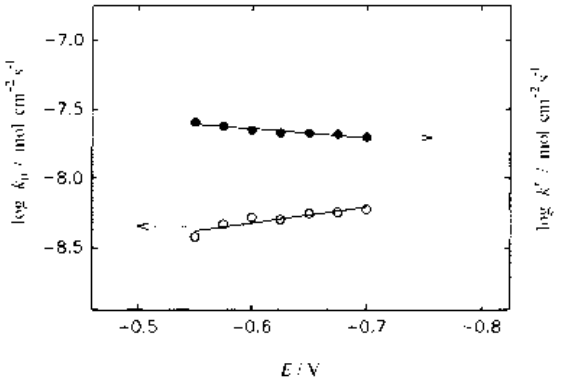

Fig. 6. Plot of $\log k_0$ (○) and $\log k'$ (●) for hard gold, determined from Equation 4, against potential applied between –0.55 V and –0.70 V.

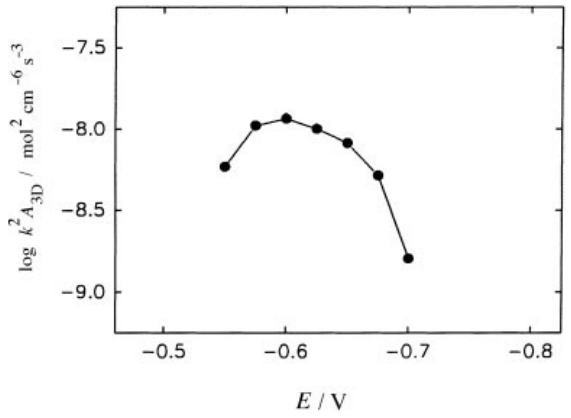

Fig. 7. Plot of log k^2A_{3D} for hard gold, determined from Equation 4, against potential applied between −0.55 V and −0.70 V.

3.3. *Morphology of the deposits*

The surface morphology of deposit depends strongly on the applied potential, deposition time, solution composition, and also preparation of the substrate. Visual inspection showed that the surface of deposit is smooth and bright when the applied potential is more positive than the peak potential on the LSVs. It becomes dull, especially at longer deposition times, as the potential is made more negative than peak potential. However, in the second potential range (characterized by current increase), the surface becomes smooth and bright again. For the purpose of comparison, gold deposits were obtained from solutions in the absence and presence of nickel to understand its influence on gold deposition.

3.3.1. Observation of morphology by SEM. First, SEM was used to observe the growth morphology of soft gold deposits in the absence of nickel. Deposition at more positive potential (–0.6 V) immediately produces a large number of small crystals with different sizes randomly distributed on the surface. Crystals are polyangular with somewhat rounded features and their grain size increases with time. No well defined surface topography was observed in the later stages, presumably due to the overlap of crystals.

Figure 8 shows an SEM of soft gold deposits at different potentials. Grain size increases as the potential changes from –0.60 V to –0.80 V. At –0.80 V, truncated pyramids are clearly shown with grain size up to about 4 μm (Fig. 8b). At –1.0 V, the surface consists of two growing phases, one with smaller grains uniformly distributed on the surface, the other with a bigger grain size up to about 1 μm formed upon the growing crystals of the first phase, Fig. 8c.

Hard gold deposited at –0.60 V forms a large number of crystals with various grain sizes which grow with time. The growth morphology looks hemispherical or pyramidal, showing some polyangular features and later the crystals overlap. At –0.75 V, the grain size decreases as compared with that obtained at –0.60 V after the same time indicating that the inhibition of growth occurs. At –1.0 V the grains are more rounded than those observed at –0.60 V.

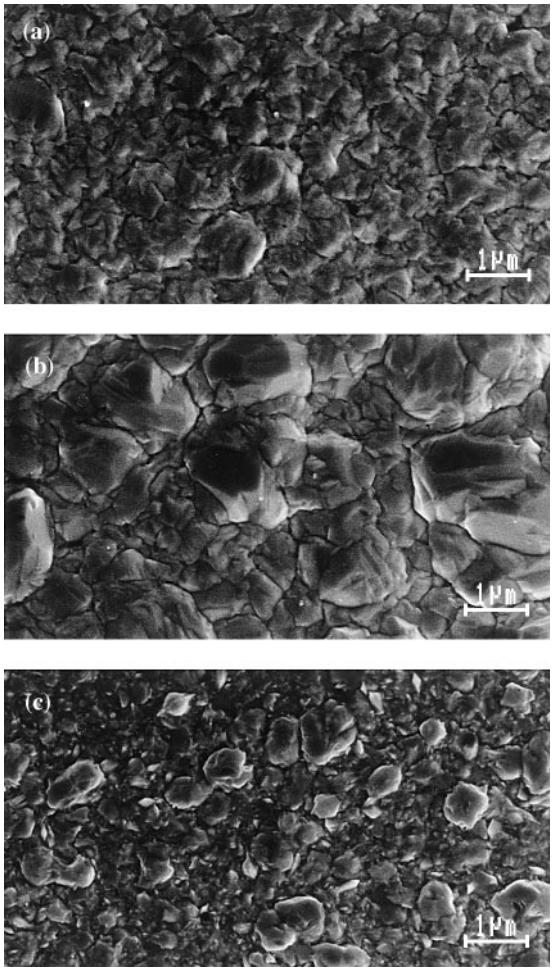

Fig. 8. SEM of soft gold deposits on Cu at different potentials: (a) −0.60 V, 600 s; (b) −0.80 V, 600 s; (c) −1.00 V, 250 s.

3.3.2. Characterization of surface morphology by AFM. In nucleation and growth studies it is important to determine the grain size, topography of growth, roughness, height of clusters, the distribution of crystal sizes, etc. Such quantitative information may be obtained from the AFM. AFM images of soft gold show that after 50 s of deposition at –0.60 V there are no important changes in the surface morphology. After 250 s, a large number of small clusters randomly distributed on the surface is formed. The grain size of clusters increases with time up to about 2 μm in lateral direction and about 50–500 nm in height after 600 s. AFM images of soft gold deposits obtained at different potentials reveal that as potential changes from –0.60 V to –0.80 V, the number of clusters decreases, while the grain size increases. The largest grains obtained at –0.80 V after 600 s of deposition are about 4 μm in lateral direction. AFM images at potentials –0.95 V and –1.0 V after 250 s of deposition show formation of rounded structures. At –1.0 V clusters have various grain sizes up to 2.4 μm, bigger than those at –0.95 V.

AFM images of hard gold deposition at –0.60 V show that at the initial stages, immediately after

minimum on current–time transients (Fig. 4) (i.e., after 50 s), cluster growth is observed; however, their shape is not well defined at this early stage. After 150 s 3D growth of crystals is observed; they are randomly distributed on the surface and become better defined at this stage. However, the separation of crystals is not good; overlap of crystals is observed even at the beginning of deposition. As deposition time increases, grain size increases. The 'roughening' of the surface may be described by the mean roughness of the surface, R_a (nm), which is calculated as [33]:

$$R_a = (L_x L_z)^{-1} \int_0^{L_x} \mathrm{d}x \int_0^{L_z} \mathrm{d}z \, f(x,z) \qquad (5)$$

where $f(x,z)$ is the surface relative to the central plane, and L_x, L_z, the horizontal and vertical dimensions of the image, relatively. Table 1 displays the mean roughness and the maximum height of grains of hard gold at –0.60 V as a function of time. The mean roughness of the deposit and the maximum height of grains increase with time. There seems to be no preferential growth on the defects, and the deposition proceeds randomly on the surface. The growth topography at a later stage (450 s) is pyramidal with different grain sizes. A similar growth pattern, that is, 3D pyramids, are observed at all potentials.

Figure 9 shows AFM images of hard gold deposits on Cu (obtained after 450 s). As the potential is made more negative from –0.50 to –0.65 V, the grain heights and their lateral sizes increase up to about 1.2 μm in the lateral direction and grains become more rounded. However, grain size seems to decrease at more negative potentials. For example, the clusters at –0.75 V are smaller than those observed at –0.65 V; their size in lateral direction is only about 500 nm, much smaller than that obtained at –0.65 V or –0.70 V, presumably indicating the growth inhibition. At –1.0 V (corresponding to the second potential range on LSV in Fig. 1), grain size again increases in comparison with that at –0.80 V. The pyramids have various sizes, indicating that such a nucleation is time-dependent, that is, a progressive one. Figure 10 shows the mean roughness and the maximum grain height of hard gold deposits obtained at potentials between –0.50 V; and –0.80 V. The mean roughness increases and surface becomes rougher with negative potential; however, at –0.80 V, the roughness again drops to a very low value. Meanwhile, the maximum grain height increases from 226 nm at –0.50 V to 728 nm at –0.70 V, and drops to 285 nm at –0.80 V. The results suggest that growth in the vertical direction is inhibited.

Table 1. Mean surface roughness, R_a, and the maximum grain height, R_{max}, for hard gold deposits on Cu at −0.60 V

Deposition time s	*50*	*150*	*400*
R_a / nm	13.1	17.4	39.3
R_{max} / nm	165.6	190.5	466.4

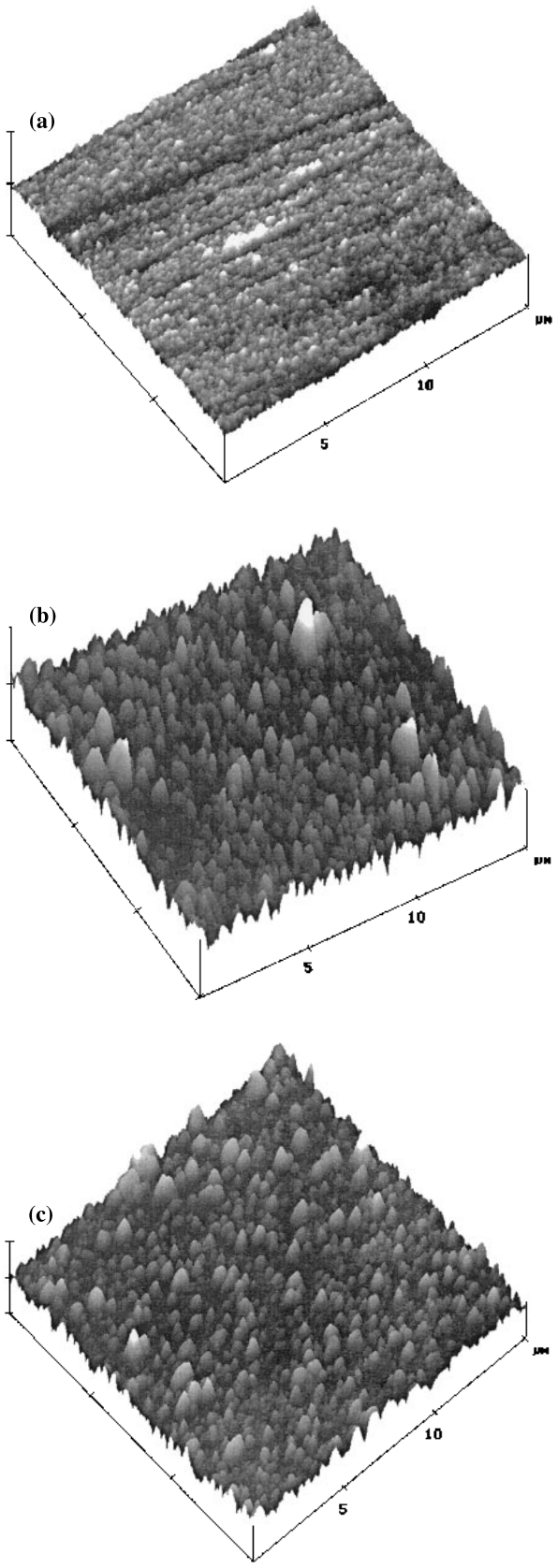

Fig. 9. Three-dimensional view AFM images of hard gold deposits on Cu at different potentials. Deposition time 450 s; potential: (a) –0.50; (b) –0.65 and (c) –0.75 V. Images are 5 μm div^{-1} for the x–y plane and 500 nm div^{-1} in the z direction.

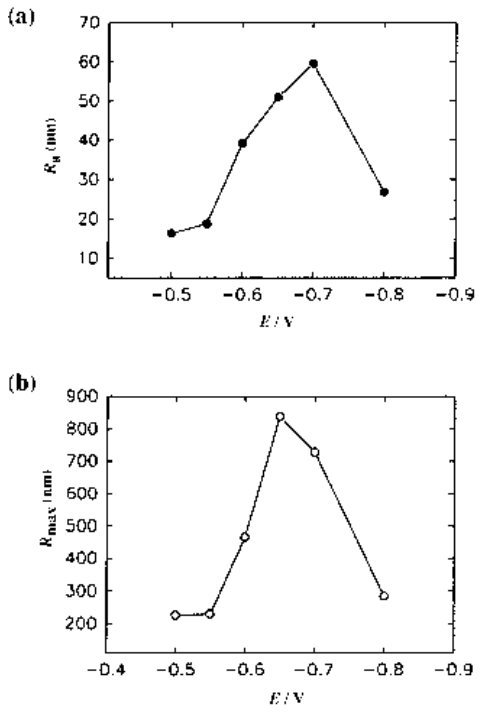

Fig. 10. The dependence of the mean surface roughness, R_a, and the maximum grain height, R_{max}, for gold deposits obtained from hard gold bath, against potential applied between −0.50 V and −0.80 V.

Figure 11 illustrates the cross sections of AFM images of hard gold deposits at –0.60 V and –0.70 V, pyramidal growth is clearly seen. The scale in z direction is greatly expanded with respect to that in x–y plane, and the shape evolution of AFM images illustrates that the growth rate in the lateral direction is nearly four times that in the vertical direction. Since all the clusters are not well separated, the values of both cluster density and the mean cluster size were not measured. The AFM lateral resolution does not provide separation of very close clusters, the result being an overestimation of the cluster size together with an underestimation of the density of clusters.

4. Discussion

LSV measurements indicate that the reaction mechanism of gold deposition on copper substrate is similar to that found on gold and other substrates. A peak-like behaviour observed at potentials between –0.5 V and –0.9 V shows an inhibition during gold deposition. From chronoamperometric measurements, it was found that the mechanism of nucleation and crystal growth of hard gold on a copper substrate at more positive potentials was similar to that obtained earlier on a gold substrate. Analysis of current–time transients shows that three-dimensional progressive nucleation and growth of right circular cones is involved in gold deposition. The crystal growth is inhibited because the vertical growth rate constant decreases with negative potential. Such inhibition is probably related to a decrease in the coverage of active species AuCN adsorbed on electrode due to the desorption of AuCN at more negative potentials.

The surface morphology of deposits was characterized using SEM and AFM. SEM showed hemispherical or pyramidal morphology with various grain sizes. The structural aspects of gold deposits from the same proprietary bath under galvanostatic mode and high speed jet plating conditions were also studied by Bocking and Cameron using SEM [20, 21], a rounded mound structure (hemispherical one) of crystal was shown to be similar to that found in this paper. The so-called ‘rounded mound structure’ was also reported by Nakahara [18] in his SEM study of cobalt hardened gold deposition. However, it is impossible to distinguish hemispherical and pyramidal growth patterns by SEM technique. It is quite evident from AFM results that the surface topography of hard gold deposits is better described by three-dimensional pyramidal growth, rather than hemispherical one. The growth rate in the lateral direction is about four times that in the vertical direction. Clusters of various sizes are randomly distributed on the surface.

SEM and AFM studies show that the number of crystals and their grain size vary with time, indicating the progressive nucleation of three-dimensional pyramids. Therefore, the model of three-dimensional progressive nucleation and growth of right circular cones found electrochemically is further confirmed by surface studies. Both techniques show that the

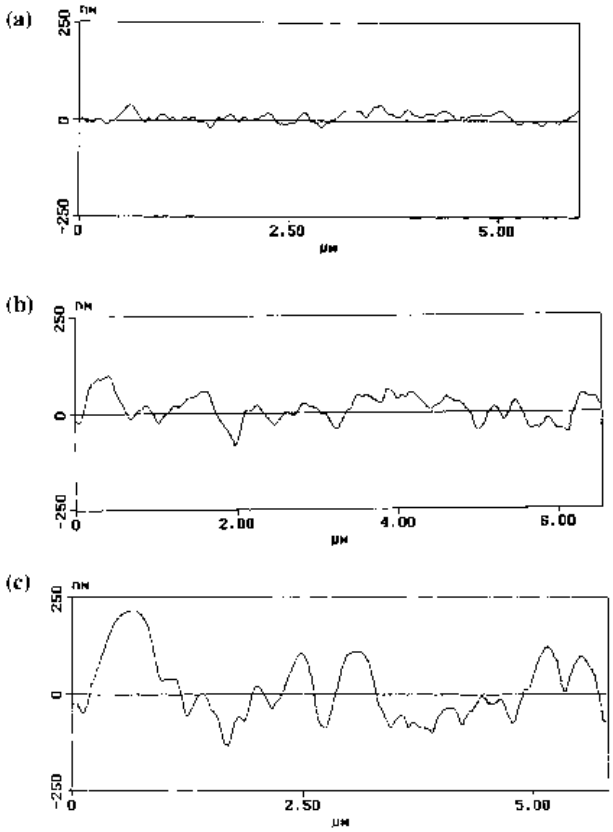

Fig. 11. Section analysis of AFM images of hard gold deposits on Cu at different potentials. Deposition time 450 s; potential: (a) −0.55, (b) −0.65 and (c) −0.70 V.

inhibition of growth is involved in gold deposition. In comparison with soft gold deposits, the crystals of hard gold are more rounded and more uniformly distributed. Furthermore, the grain sizes of hard gold deposits are much smaller due to the addition of nickel in the bath, resulting in fine-grained deposits. Nickel appears to act as a grain refiner as well as a hardener.

5. Conclusions

Gold deposits on copper substrate from citrate-based proprietary solution were characterized by linear sweep voltammetry, chronoamperometry, SEM and AFM techniques. The mechanism and kinetics of nucleation and growth of hard gold were determined chronoamperometrically. It was found that three-dimensional progressive nucleation and growth of right-circular cones describes the experimental data well. It was also shown that the inhibition of crystal growth occurs in gold deposition.

The surface morphology of gold deposits was characterized using SEM and AFM techniques. The inhibition of crystal growth observed electrochemically was further confirmed by SEM and AFM measurements. The height, growth morphology, grain size, roughness were determined using AFM. It was found that hard gold deposits form three-dimensional pyramids. The mean surface roughness and the maximum grain height increase with time, and these values also increase with negative potential from –0.50 to –0.75 V, and, subsequently, they decrease steeply after –0.80 V due to the inhibition of growth.

Acknowledgements

The authors thank Dr L. Chen and Prof. D. Guay from INRS Energy and Materials for their help in preparing AFM images. Financial support from NSERC is gratefully acknowledged.

References

[1] I. R. Christie and B. P. Cameron, *Gold Bull.* **27** (1994) 12.
[2] R. T. Page, *Metal Finish. J.* **20** (1974) 4.
[3] F. R. Schlodder, H. H. Beyer and W. G. Zilske, *in* 'GOLD 100', Proceedings of the International Conference on Gold (Proceedings of the Symposium on the Industrial Uses of Gold), Vol. **3** Johannesburg (1986), p. 21.
[4] W. T. Lee, *Corros. Technol.* **10** (1963) 59.
[5] J. A. Lochet, Proc. 77th AESF Annual Technical Conference (1990), p. 983.
[6] J. Hendriks, *in* 'Connectors 91', One day Symp. Exhib. (edited by G. D. Wilox and D. H. Ross), Inst. Met. Finish., Birmingham (1991), p. 20.
[7] I. R. Christie, *in* 'Connectors 91' *op. cit.* [6], p. 61.
[8] V. N. Fedorova and B. S. Krasikov, *Zh. Prikl. Khim.* **50** (1977) 792.
[9] H. R. Khan, M. Baumgartner and C. J. Raub, *in* Proceedings of the Symposium on Electrodeposition Technology: Theory and Practice, The Electrochemical Society, Pennington NJ (1987), p. 165.
[10] S. J. Hemsley and R. V. Green, *Trans. Inst. Metal Finish.* **69** (1991) 149.
[11] P. Bindra, D. Light, P. Freudenthal and D. Smith, *J. Electrochem. Soc.* **136** (1989) 3616.
[12] E. T. Eisenmann, *ibid.* **125** (1978) 717.
[13] N. N. Balashova, T. A. Smirnova, N. A. Smagunova and A. K. Yudina, *Zh. Prikl. Khim.* **50** (1977) 2698.
[14] H. Angerer and N. Ibl, *J. Appl. Electrochem.* **9** (1979) 219.
[15] J. M. Leeds and M. Clarke, *Trans. Inst. Metal Finish.* **47** (1969) 163.
[16] R. M. Krishnan, S. Sriveeraraghavan and S. R. Natarajan, *Metal Finish.* **86** (1988) 56.
[17] D. Davidovic and R. R. Adzic, *Electrochim. Acta* **33** (1988) 103.
[18] S. Nakahara, *J. Cryst. Growth* **75** (1986) 212.
[19] Y. Okinaka and S. Nakahara, *J. Electrochem. Soc.* **123** (1976) 1284.
[20] C. Bocking and B. Cameron, *Trans*, *Inst. Met. Finish.* **72** (1994) 33.
[21] C. Bocking and C. Dineen, *ibid.* **72** (1994) 101.
[22] Y. Okinaka, *in* Proceedings of the Symposium on Electrodeposition Technology: Theory and Practice, The Electrochemical Society, Pennington NJ (1987), p. 148.
[23] W. Chrzanowski, Y. G. Li and A. Lasia, *J. Appl. Electrochem.* **26** (1996) 385.
[24] Y. G. Li, Chrzanowski, and A. Lasia, *ibid.* **26** (1996) 843.
[25] Y. G. Li and A. Lasia, *ibid.* **26** (1996) 853.
[26] S. Manne, P. K. Hansma, J. Massie, V. B. Elings and A. A. Gewirth, *Science* **251** (1991) 183.
[27] R. M. Rynders a and R. C. Alkire, *J. Electrochem. Soc.* **141** (1994) 1166.
[28] J. R. LaGraff and A. A. Gewirth, *J. Phys. Chem.* **98** (1994) 11246.
[29] M. Koinuma and K. Uosaki, *Electrochim. Acta* **40** (1995) 1345.
[30] R. J. Nichols, D. Schröer and H. Meyer, *ibid.* **40** (1995) 1479.
[31] N. Ikemiya, S. Miyaoka and S. Hara, *Surf. Sci.* **327** (1995) 261.
[32] S. A. Hendricks, Y. T. Kim and A. J. Bard, *J. Electrochem. Soc.* **139** (1992) 2818.
[33] K. Kowal, L. Xie, R. Huq and G. C. Farrington, *ibid.* **141** (1994) 1166.
[34] E. Gomez, E. Valles, P. Gorostiza, J. Servat and F. Sanz, *ibid.* **142** (1995) 4091.
[35] N. M. Martyak and R. J. Nichols, Proc. AESF 81st Annual Technical Conference (1994), p. 561.
[36] G. Wouters, M. Bratoeva, J. -P. Celis, J. R. Roos, *Electrochim. Acta* **40** (1995) 1434.
[37] L. Chen and D. Guay, *J. Electrochem. Soc.* **141** (1994) L43.
[38] E. B. Budevski, *in* 'Comprehensive Treatise of Electrochemistry', Vol. 7, (edited by B. E. Conway, J. O'M. Bockris, E. Yeager, S. U. M. Khan and R. E. White) Plenum, London (1983), p. 399 and references therein.